

Oscillatory angular dependence of the magnetoresistance in a topological insulator $\text{Bi}_{1-x}\text{Sb}_x$

A. A. Taskin, Kouji Segawa, and Yoichi Ando

Institute of Scientific and Industrial Research, Osaka University, Ibaraki, Osaka 567-0047, Japan

The angular-dependent magnetoresistance and the Shubnikov-de Haas oscillations are studied in a topological insulator $\text{Bi}_{0.91}\text{Sb}_{0.09}$, where the two-dimensional (2D) surface states coexist with a three-dimensional (3D) bulk Fermi surface (FS). Two distinct types of oscillatory phenomena are discovered in the angular-dependence: The one observed at lower fields is shown to originate from the surface state, which resides on the $(2\bar{1}\bar{1})$ plane, giving a new way to distinguish the 2D surface state from the 3D FS. The other one, which becomes prominent at higher fields, probably comes from the (111) plane and is obviously of unknown origin, pointing to new physics in transport properties of topological insulators.

PACS numbers: 71.18.+y, 72.25.-b, 73.25.+i, 85.75.-d

The three-dimensional (3D) topological insulator hosts a novel surface state whose existence is guaranteed by a topological principle characterized by the Z_2 invariant [1–3], which makes it an interesting playground for exploring the role of topology in condensed matter [4–20]. The key feature of the topological insulator is that an odd number of massless, spin-helical Dirac cones comprise the 2D surface state, whose gapless nature is protected by the time-reversal symmetry. Such an intrinsically conducting surface is supported by an insulating bulk, where the energy gap is created by a strong spin-orbit coupling. To understand the macroscopic properties of this novel surface state and to investigate the possibility of its device applications, transport studies are obviously important. However, in actual samples of topological insulators, there is always some bulk conductivity due to residual carriers, and separating the contributions from 2D and 3D states turns out to be challenging [13–15].

Recently, we observed [13] strong de Haas-van Alphen (dHvA) oscillations in high-quality bulk single crystals of $\text{Bi}_{1-x}\text{Sb}_x$ alloy in the “insulating” regime ($0.07 \leq x \leq 0.22$), which is the first material to be known as a 3D topological insulator [2, 7]. The dHvA oscillations signified a previously-unknown Fermi surface (FS) with a clear 2D character that coexists with a 3D bulk FS [13]. Since $\text{Bi}_{1-x}\text{Sb}_x$ is a 3D material, the observed 2D FS is naturally assigned to the surface. In the present work, to specifically probe low-dimensional properties of this material, we have extended our study to the angular dependence of the magnetoresistance. This method was successfully applied to the studies of quasi-2D organic conductors in the 1980s, resulting in the discovery of the celebrated angular-dependent magnetoresistance oscillations (AMRO) [21–23], and later extended to quasi-one-dimensional conductors [24, 25]. In this Letter, we present a detailed study of the magnetotransport in a $\text{Bi}_{0.91}\text{Sb}_{0.09}$ single crystal, where we have found oscillatory angular dependences in both the resistivity ρ_{xx} and the Hall resistivity ρ_{yx} . The oscillatory magnetoresistance (MR) is obviously different from known AMRO

[25], and it is comprised of two components: one is a peculiar manifestation of the 2D FS, and the other appears to be a fundamentally new effect. The former provides a new way to distinguish the contributions of the 2D FS, while the latter points to new physics in topological insulators.

High-quality $\text{Bi}_{1-x}\text{Sb}_x$ crystals were grown from a stoichiometric mixture of 99.9999% purity Bi and Sb elements by a zone melting method [13]. The resistivity was measured by a standard four-probe method on a rectangular sample. In this Letter, we focus on a $x = 0.09$ sample in which the current was directed along the C_1 axis. Continuous rotations of the sample in constant magnetic fields was used to measure the angular dependence of the MR within two main crystallographic planes (C_3 - C_2 and C_3 - C_1). To observe the SdH oscillations, $\rho_{xx}(B)$ and $\rho_{yx}(B)$ were also measured by sweeping B between +14 and -14 T along a set of magnetic-field directions.

Let us start by presenting our main observations. Figure 1(a) shows the angular dependences of the transverse MR measured in magnetic fields rotated within the trigonal-binary (C_3 - C_2) plane perpendicular to the current. The magnetic-field strength, ranging from 0.01 T to 16 T, were kept constant during each rotation. As clearly seen in Figs. 1–3, pronounced oscillations of both ρ_{xx} and ρ_{yx} as a function of the rotation angle θ appear for $B \gtrsim 1$ T. Two different types of oscillations can be distinguished: The first type consists of oscillations appearing at lower fields (Figs. 1 and 2), while the second one becomes prominent at higher fields (Figs. 1 and 3). These data were taken immediately after the sample surface was refreshed by a chemical etching [26].

Figure 2 magnifies the “low-field” oscillations of $\rho_{xx}(\theta)$, which become prominent above 1 T. These oscillations are symmetric with respect to the C_3 axis ($\theta = 0^\circ$) and show a clear tendency of shifting the peak positions closer to the center with increasing magnetic field. It is important to notice that this strong field dependence is very different from ordinary AMRO [23] where the angular positions of peaks are determined by commensurate mo-

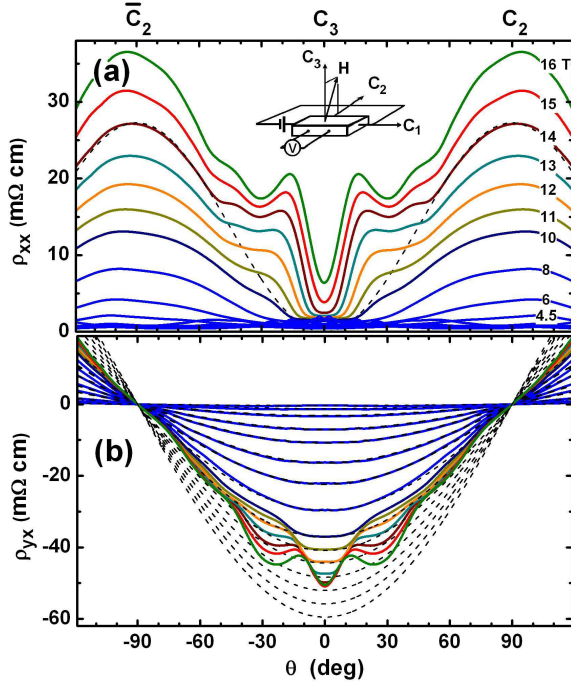


FIG. 1: (Color online) (a) Angular dependences of ρ_{xx} measured in the trigonal-binary (C_3 - C_2) plane in constant magnetic fields. The dashed line is the MR background $\sim (1 - \cos^2 \theta)$ for $B = 14$ T. Inset depicts the measurement geometry, where $\theta = 0^\circ$ corresponds to the C_3 axis. (b) Angular dependences of ρ_{yx} measured in the same conditions as in (a). The dashed lines are the expected angular dependences of the Hall effect plotted for all magnetic fields (0.1, 0.25, 0.5, 1, 2, 3, 4.5, 6, 8, 10, 11, 12, 13, 14, 15, and 16 T).

tions of electrons for certain field directions on warped FSs [24, 25] and, thus, are field-independent. Peculiarly, the amplitude of observed oscillations decrease with increasing field above ~ 8 T and disappear at higher fields. It turns out that the angular positions of the outer-most peaks (with respect to $\theta = 0^\circ$), which are marked by arrows in Fig. 2, follow a simple geometrical law (inset of Fig. 2) related to the response of the 2D electrons residing on the $(2\bar{1}\bar{1})$ plane perpendicular to the C_1 axis, as will be discussed later. Note that, because of the crystal symmetry, there are three equivalent C_1 axes in the plane perpendicular to the trigonal (C_3) axis; hence, two of the three equivalent 2D FSs are at $\pm 30^\circ$ to the rotation plane. The $\rho_{xx}(\theta)$ measurements of the same sample in magnetic fields rotated within the trigonal-bisectrix (C_3 - C_1) plane (not shown) reveal essentially similar angular dependences.

In contrast to these “low-field” oscillations, the “high-field” angular dependence of the transverse MR is developing on a smooth field-dependent background coming from the anisotropy of $\rho_{xx}(B)$ along the different axes. An example of its fitting for $B = 14$ T is shown by the dashed line in Fig. 1(a). Because of a large MR background in strong magnetic fields, only largest peaks in

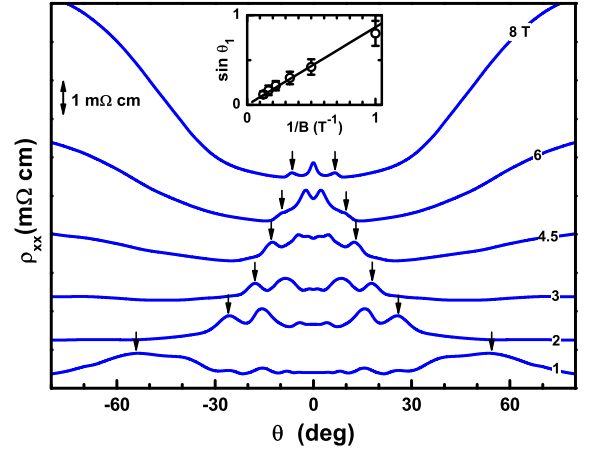


FIG. 2: (Color online) “Low-field” angular dependences of ρ_{xx} shown in Fig 1(a). Curves are shifted for clarity. Arrows mark the positions of the first peaks, which appear as the field direction is rotated from the C_2 (\bar{C}_2) to C_3 axis. Inset shows the dependence of θ_1 on B plotted as $\sin \theta_1$ vs B^{-1} , which gives evidence for the 2D-FS origin of the peaks.

$\rho_{xx}(\theta)$ can be clearly seen in the raw data [Fig. 1(a)]. Subtracting the background would help to reveal smaller peaks, but it is not necessary, because the situation is much simpler in the Hall data as shown below.

Figure 1(b) shows the $\rho_{yx}(\theta)$ data, which also show pronounced angular-dependent oscillations at high fields. The “background” for $\rho_{yx}(\theta)$ is simply the angular dependence of the Hall effect, $R_H B \cos \theta$, where R_H is the Hall coefficient. As can be clearly seen in Fig. 1(b), low-field $\rho_{yx}(\theta)$ data follow this expected angular dependence very closely (we use $R_H = -37 \text{ cm}^2/\text{C}$, obtained from the Hall measurements), and the large deviation from this simple behavior is observed only in magnetic fields above 10 T. Figure 3 shows “pure” oscillations in $\Delta \rho_{yx}(\theta)$ after subtracting the $R_H B \cos \theta$ contribution from $\rho_{yx}(\theta)$. One can clearly see a set of peaks, which are marked by short vertical ticks in Fig. 3. They are symmetric with respect to the C_3 axis and show a rather complicated magnetic-field dependence.

To understand the origin of the observed angular-dependent oscillations, detailed knowledge of the FS is useful. We therefore measured the SdH oscillations on the present sample for a series of magnetic-field directions in two high-symmetry planes, as shown in Fig. 4(a) for the C_3 - C_1 plane. Those SdH oscillations consist of three fundamental frequencies, which we call f_1 , f_2 , and f_3 . How these frequencies vary in the C_3 - C_1 plane is shown in Fig. 4(b), which is essentially consistent with what was observed with the dHvA oscillations [13] and indicates the presence of both 2D and 3D FSs. In the present sample, the radius of the circular 2D FS (given by f_1) is $k_F = 4.15 \times 10^5 \text{ cm}^{-1}$ which is the same as in Ref. 13, while the 3D FS is somewhat smaller, the semi-axes of the three ellipsoidal 3D FSs (given by f_2 and

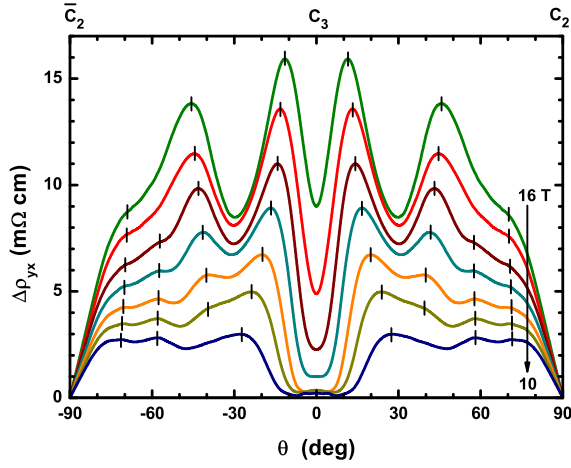


FIG. 3: (Color online) “High-field” angular-dependent oscillations of $\Delta\rho_{yx}$ obtained by subtracting the expected $R_H B \cos\theta$ behavior from the ρ_{yx} data shown in Fig. 1(b). Ticks mark the positions of distinguishable peaks.

f_3) are $a = 1.2 \times 10^6 \text{ cm}^{-1}$, $b = 8.5 \times 10^5 \text{ cm}^{-1}$, and $c = 4.2 \times 10^5 \text{ cm}^{-1}$. Note that the 2D FS resides on the plane perpendicular to the C_1 axis, while the 3D ellipsoids are located at the L points of the bulk Brillouin zone, with the longest axes in the binary plane and tilted from the C_1 axis by $\sim 5^\circ$. The divergence of f_1 at $\theta = 0^\circ$ seen in Fig. 4(b) is of geometric origin and is a hallmark of the 2D FS, as can be seen in the inset of Fig. 4(b).

The analysis of the SdH amplitude gives us the cyclotron mass m_c and the scattering time τ . For the field direction very close to the C_3 axis, the SdH oscillations coming from the 2D and 3D FSs can be easily separated, and their fits to the standard Lifshitz-Kosevich theory [27] at $\theta \approx 3^\circ$ yield m_c/m_e of 0.13 and 0.033 for the 2D and 3D FSs, respectively (m_e is the free electron mass). Note that the relatively large m_c for the 2D FS originates from its characteristic angular dependence $m_c = m_c^0/\sin\theta$, where $m_c^0 = 0.0057m_e$ is for the orbital motion in perpendicular fields ($B \parallel C_1$), meaning that the 2D electrons are actually extremely light. Corresponding Dingle plots (not shown) give Dingle temperatures T_D of about 5.5 K and 7 K for the 2D and 3D FSs, which imply the mean free paths of $l^{2D} \approx 150 \text{ nm}$ and $l^{3D} \approx 16 \text{ nm}$, respectively [28]. This difference is not surprising, if one remembers the Dirac nature [29, 30] of the 2D surface states and that they are topologically protected against spin-conserving backscattering.

We now discuss the origin of the “low-field” part of the angular-dependent oscillations in $\text{Bi}_{0.91}\text{Sb}_{0.09}$. A key insight comes from the recognition that the 3D FSs in our sample enter the quantum limit (where all the electrons condense into the first Landau level) with magnetic fields of only 1–3 T for any direction, while the necessary magnetic field to bring the 2D FS into the quantum limit diverges as the field direction is rotated toward the C_3

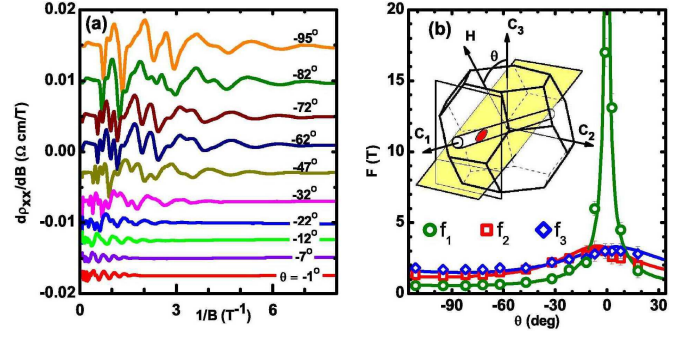


FIG. 4: (Color online) (a) SdH oscillations measured in the C_3 - C_1 plane. For better visibility, $d\rho_{xx}/dB$ is calculated after a smooth background MR is subtracted, and the curves are shifted. (b) θ -dependences of the three fundamental frequencies obtained from the Fourier transform of the SdH oscillations. Inset shows a schematic picture of the bulk Brillouin zone, in which the 2D FS is crossed by a plane perpendicular to the magnetic-field direction.

axis. This means that, in sufficiently high magnetic field, the 3D electrons will always remain in the quantum limit, while the 2D electrons can always be brought from the quantum limit back to the regime where higher Landau levels are populated. This will lead to the oscillating behavior of ρ_{xx} due to the 2D FS alone when the magnetic field is rotated toward the C_3 axis. Remembering that the resistivity oscillates as $\rho_{xx} \sim \cos[2\pi(F/B_{\text{eff}} + \gamma)]$ with $B_{\text{eff}} = B \sin\theta$, a maximum in ρ_{xx} occurs when $F/B_{\text{eff}} + \gamma = n$ with integer n . Hence, one can understand that the Fermi level is crossed by the n -th Landau level of the 2D FS at the specific angle θ_n given by

$$\theta_n = \arcsin\left(\frac{F/B}{n - \gamma}\right), \quad (1)$$

where F is the frequency and γ is the phase of the SdH oscillations. According to this model, the outer-most peaks marked by arrows in Fig 2 are coming from the crossing of the Fermi level by the first Landau level ($n = 1$) at a given magnetic-field strength, so their angles should correspond to θ_1 . Actually, the inset of Fig. 2 demonstrates that Eq. (1) fits the data reasonably well. If F is assumed to be 0.65 T based on the SdH result [31], the fit in Fig 2 yields γ of 0.25, suggesting a non-zero Berry phase associated with the 2D FS [32, 33].

Finally, let us discuss the origin of the “high-field” peaks shown in Figs. 1 and 3. Here, an important feature is that the amplitude of these peaks weakens as the magnetic field is rotated away from the C_3 axis, which is somewhat reminiscent of the behavior of the ordinary AMRO in quasi-2D systems if the conduction planes lie perpendicular to the C_3 axis [21–23]. Note that this is different from what is observed for the “low-field” oscillations, which are originating from the surface state residing on the $(2\bar{1}\bar{1})$ plane ($\perp C_1$). Thus, it is probable that the “high-field” oscillations are coming from the (111)

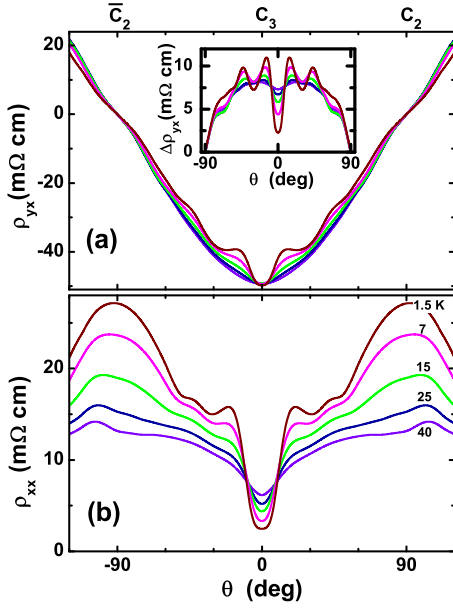


FIG. 5: (Color online) (a) Angular-dependent oscillations of ρ_{yx} within the C_3 - C_2 plane in the constant field $B = 14$ T measured at 1.5, 7, 15, 25, and 40 K. Inset shows oscillations of $\Delta\rho_{yx}$ after subtraction of the $R_H B \cos \theta$ term. (b) Angular-dependent oscillations of ρ_{xx} within the C_3 - C_2 plane measured in the same conditions as in (a).

plane ($\perp C_3$), where surface states are seen in photoemission [7–10] and tunneling [11] experiments. Another distinguishable feature of the “high-field” oscillations is that they survive up to rather high temperatures as can be seen in Fig. 5, where temperature dependences of both $\rho_{yx}(\theta)$ and $\rho_{xx}(\theta)$ are shown. Even at 40 K there are still visible traces of oscillations (see the inset of Fig. 5), while the “low-field” SdH and angular-dependent oscillations disappear around 20 K. In spite of some similarities to the quasi-2D AMRO, the peak positions of the “high-field” oscillations apparently shift with the magnetic field, which is not expected for the ordinary AMRO. Moreover, the existence of a finite coupling between conduction planes is essential for the quasi-2D AMRO [25], but there is no such inter-plane coupling for the surface states as long as the crystal is thick enough. Therefore, the observed “high-field” angular oscillations are a new phenomenon apparently specific to topological insulators, and it is possible that they are associated with a coupling between the surface and the bulk states.

In conclusion, we found two different types of oscillatory phenomena in the angular-dependent MR of a topological insulator $\text{Bi}_{0.91}\text{Sb}_{0.09}$. One type is observed at lower fields and provides a new way to distinguish the 2D FS. The other one, which becomes prominent at higher fields, probably comes from the (111) plane and points to new physics in transport properties of topological insulators.

We thank V. M. Yakovenko for discussions. This

work was supported by JSPS (KAKENHI 19674002 and 20030004) and AFOSR (AOARD 08-4099 and 10-4103).

-
- [1] L. Fu, C. L. Kane, and E. J. Mele, Phys. Rev. Lett. **98**, 106803 (2007).
 - [2] L. Fu and C. L. Kane, Phys. Rev. B **76**, 045302 (2007).
 - [3] J. E. Moore and L. Balents, Phys. Rev. B **75**, 121306(R) (2007).
 - [4] X-L. Qi, T. L. Hughes, and S.-C. Zhang, Phys. Rev. B **78**, 195424 (2008).
 - [5] J. C. Y. Teo, L. Fu, and C. L. Kane, Phys. Rev. B **78**, 045426 (2008).
 - [6] H.-J. Zhang *et al.*, Phys. Rev. B **80**, 085307 (2009).
 - [7] D. Hsieh *et al.*, Nature **452**, 970 (2008).
 - [8] D. Hsieh *et al.*, Science **323**, 919 (2009).
 - [9] D. Hsieh *et al.*, Nature **460**, 460 (2009).
 - [10] A. Nishide *et al.*, Phys. Rev. B **81**, 041309(R) (2010).
 - [11] P. Roushan *et al.*, Nature **460**, 1106 (2009).
 - [12] T. Zhang *et al.*, Phys. Rev. Lett. **103**, 266803 (2009).
 - [13] A. A. Taskin and Y. Ando, Phys. Rev. B **80**, 085303 (2009).
 - [14] H. Peng *et al.*, Nature Materials, doi:10.1038/nmat2609.
 - [15] J. G. Checkelsky *et al.*, Phys. Rev. Lett. **103**, 246601 (2009).
 - [16] R. Shindou and S. Murakami, Phys. Rev. B **79**, 045321 (2009).
 - [17] A. P. Schnyder, S. Ryu, A. Furusaki, and A. W. W. Ludwig, Phys. Rev. B **78**, 195125 (2008).
 - [18] Y. Tanaka, T. Yokoyama, and N. Nagaosa, Phys. Rev. Lett. **103**, 107002 (2009).
 - [19] Y. Ran, Y. Zhang, and A. Vishwanath, Nat. Phys. **5**, 298 (2009).
 - [20] D.-H. Lee, Phys. Rev. Lett. **103**, 196804 (2009).
 - [21] M. V. Kartsovnik *et al.*, JETP Lett. **48**, 541 (1988).
 - [22] K. Kajita *et al.*, Solid St. Comm. **70**, 1189 (1989).
 - [23] K. Yamaji, JPSJ **58**, 1520 (1989).
 - [24] G. M. Danner, W. Kang, and P. M. Chaikin, Phys. Rev. Lett. **72**, 3714 (1994).
 - [25] B. K. Cooper and V. M. Yakovenko, Phys. Rev. Lett. **96**, 037001 (2006).
 - [26] We observed weaker oscillations in the same sample before etching, corroborating their surface origin.
 - [27] D. Schoenberg, *Magnetic Oscillations in Metals* (Cambridge University Press, 1984).
 - [28] The scattering time τ ($= \hbar/2\pi k_B T_D$) and the Fermi velocity v_F ($= \hbar k_F/m_c$) gives the mean free path $\ell = v_F \tau$. In the present sample, $v_F^{3D} \approx 7.6 \times 10^6$ cm/s is an order of magnitude smaller than $v_F^{2D} \approx 8.4 \times 10^7$ cm/s.
 - [29] S. G. Sharapov, V. P. Gusynin, and H. Beck, Phys. Rev. B **69**, 075104 (2004).
 - [30] V. P. Gusynin and S. G. Sharapov, Phys. Rev. B **71**, 125124 (2005).
 - [31] The SdH frequency of the 2D FS is 0.57 T when B is perpendicular to the 2D plane, but it becomes 0.65 T when B is 30° tilted, as is the case for two of the three equivalent 2D FSs in $B \parallel C_2$.
 - [32] G. P. Mikitik and Yu. V. Sharlai, Phys. Rev. Lett. **82**, 2147 (1999).
 - [33] Y. Zhang *et al.*, Nature **438**, 201 (2005).